Electronic Supplementary Material (ESI) for Journal of Materials Chemistry A.
This journal is © The Royal Society of Chemistry 2022

Electronic Supplementary Information

Construction of plasmonic 1T-WS_2/2H-WS_2/CdS heterostructures for enhanced solar driven hydrogen evolution

Xiaoyu Chen, Zhi Han, Bin Zhang*, Bojing Sun, Yu Wang, Yunchen Du, Xijiang Han*, and Ping Xu*

MIIT Key Laboratory of Critical Materials Technology for New Energy Conversion and Storage, School of Chemistry and Chemical Engineering, Harbin Institute of Technology, Harbin 150001, China

Email: pxu@hit.edu.cn (P.X.); zhangbin_hit@aliyun.com; hanxijiang@hit.edu.cn (X.H.)

Contents

Table. S5 Time-resolved PL decay curve parameters obtained by double-exponential function simulation.

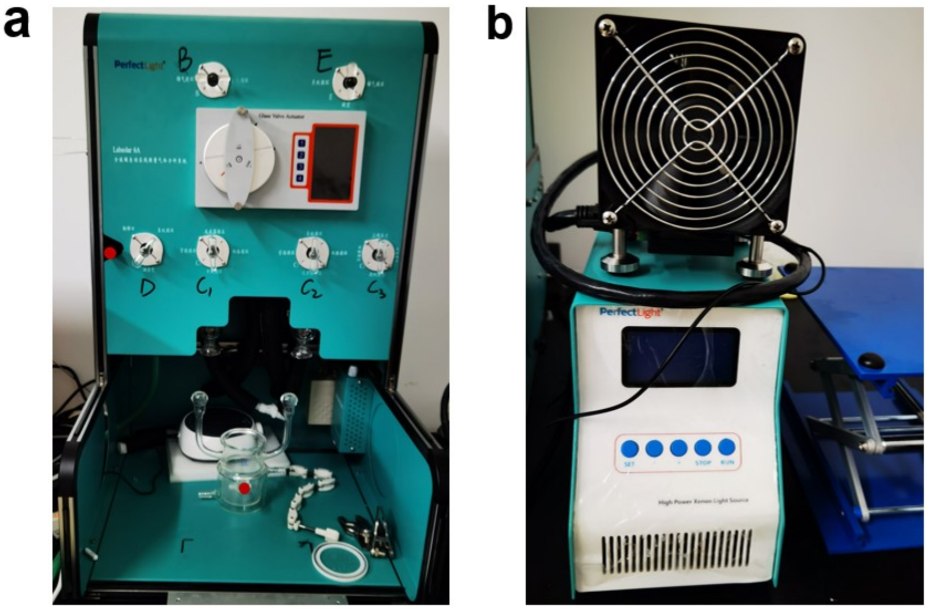

Fig. S1. (a) PerfectLight Labsolar 6A and (b) PerfectLight PLS-SXE300/300UV.

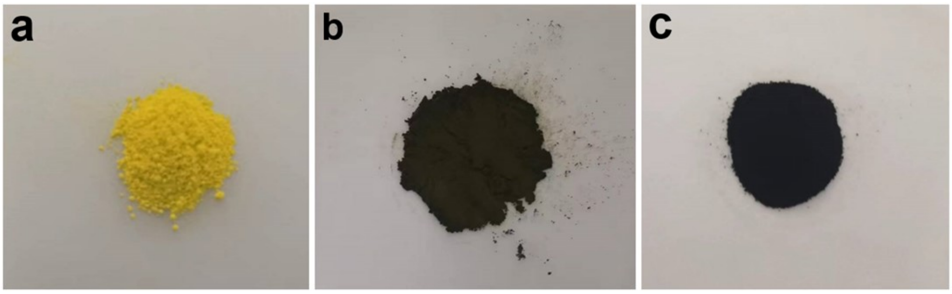

Fig. S2. Optical images of (a) pure CdS nanorods, (b) 1T-WS_2/2H-WS_2/CdS heterostructures (WWC-1-6), and (c) pure WS_2 nanosheets.

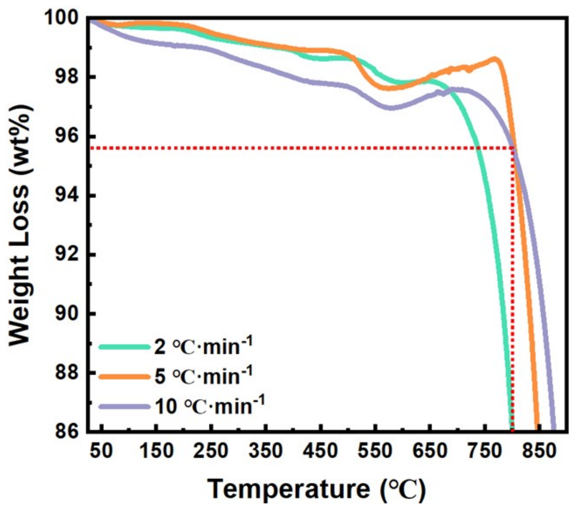

Fig. S3. TG curves of pure CdS nanorods under N_2 atmosphere.

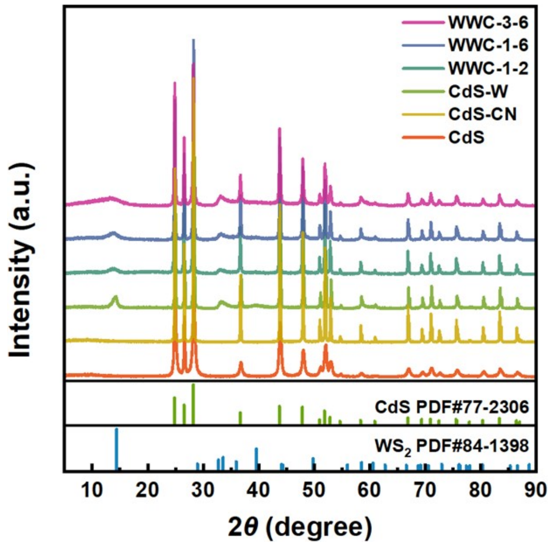

Fig. S4. XRD patterns of different 1T-WS_2/2H-WS_2/CdS heterostructures (WWC-3-6, WWC-1-6, WWC-3-2), CdS-W (CdS-W represents only calcination the mixture of CdS and $H_{28}N_6O_{41}W_{12}\cdot H_2O$ after grinding), CdS-CN (CdS-CN represents only calcination the mixture of CdS and $C_2H_4N_4$ after grinding), and pure CdS nanorods.

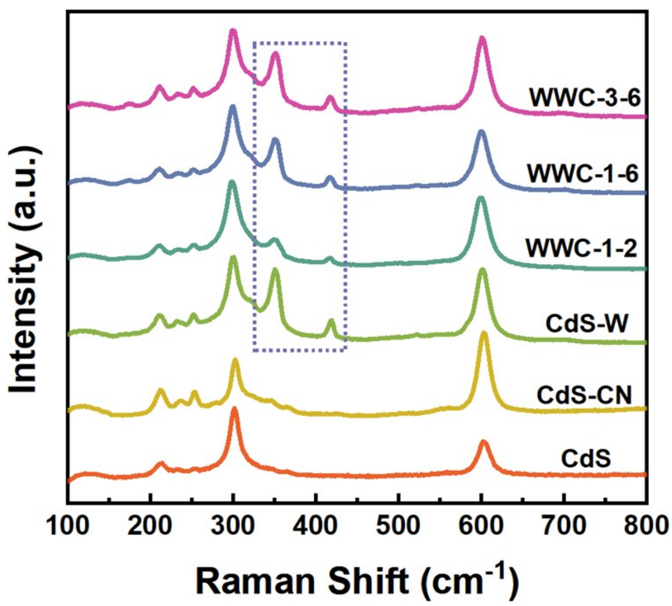

Fig. S5. Raman spectra of different 1T-WS_2/2H-WS_2/CdS heterostructures (WWC-3-6, WWC-1-6, WWC-1-2), CdS-W (CdS-W represents only calcination the mixture of CdS and $H_{28}N_6O_{41}W_{12}\cdot H_2O$ after grinding), CdS-CN (CdS-CN represents only calcination the mixture of CdS and $C_2H_4N_4$ after grinding), and pure CdS nanorods.

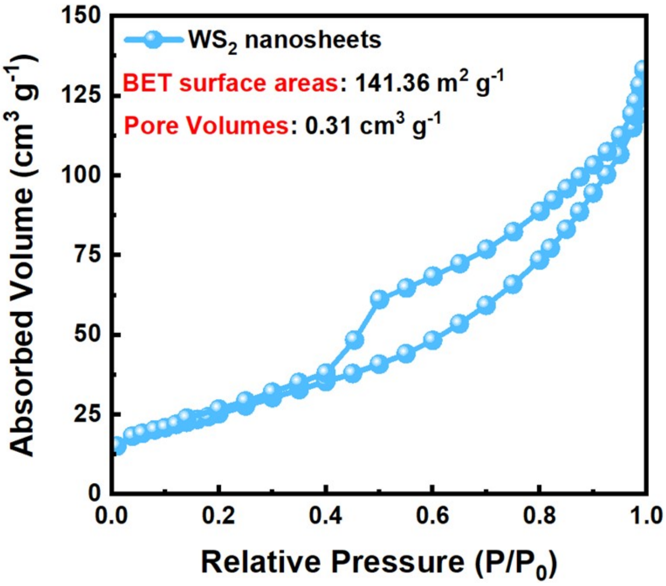

Fig. S6. Nitrogen sorption isotherms, BET surface areas, and pore volumes of pure WS_2 nanosheets.

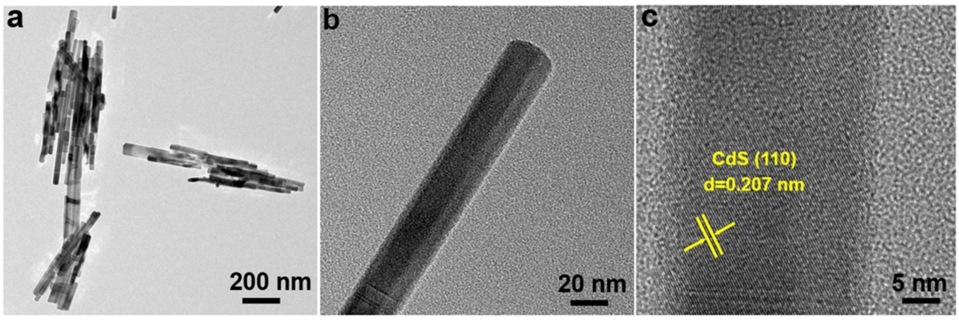

Fig. S7. TEM and HRTEM images of pure CdS nanorods.

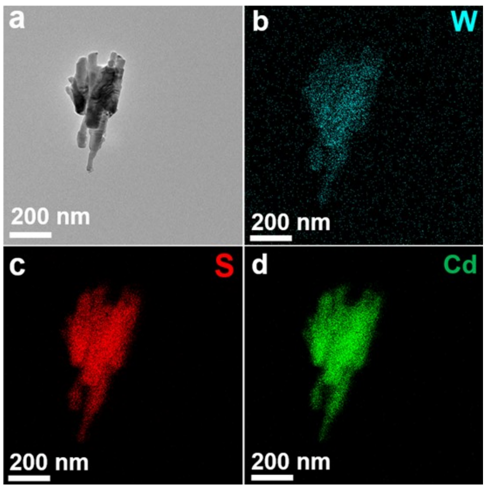

Fig. S8. TEM and the corresponding EDX mapping images of CdS-W heterostructures (CdS-W represents only calcination the mixture of CdS and $H_{28}N_6O_{41}W_{12}{\cdot}H_2O$ after grinding).

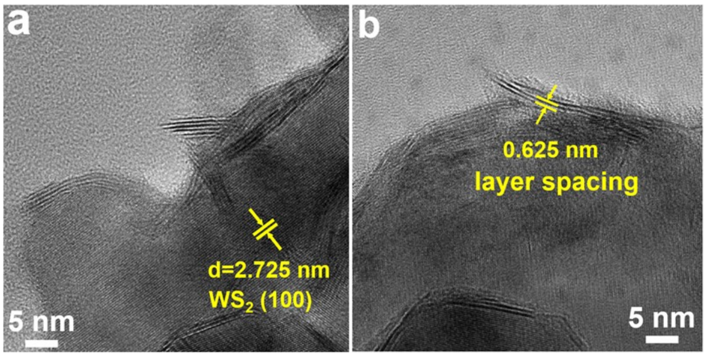

Fig. S9. HRTEM images of pure WS_2 nanosheets.

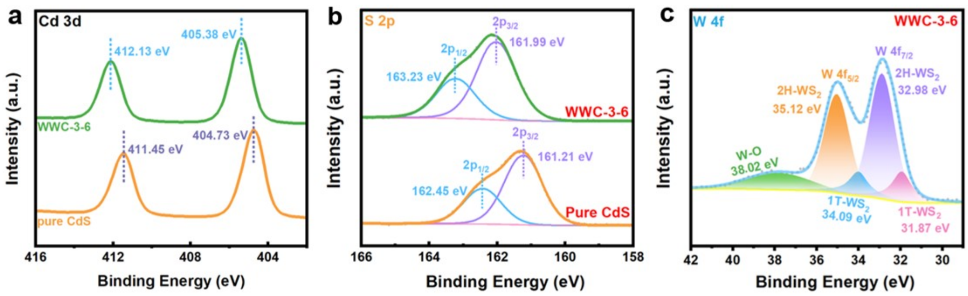

Fig. S10. Comparison diagram of (a) Cd 3d, (b) S 2p, and (c) W 4f of 1T-WS_2/2H-WS_2/CdS heterostructures (WWC-3-6).

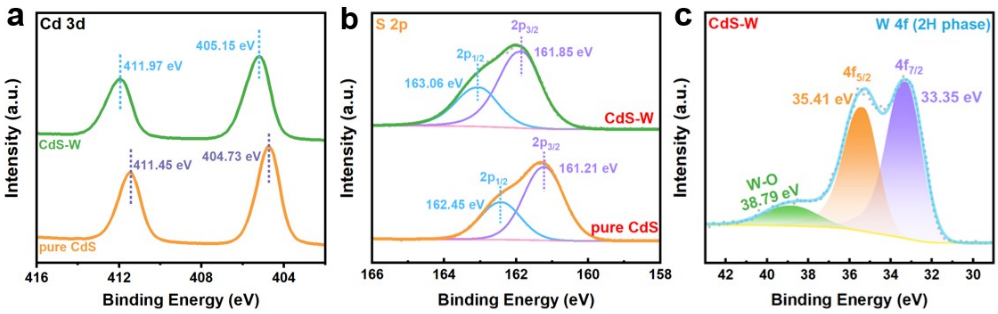

Fig. S11. Comparison diagram of (a) Cd 3d, (b) S 2p, and (c) W 4f of CdS-W heterostructures (CdS-W represents only calcination the mixture of CdS and $H_{28}N_6O_{41}W_{12}·H_2O$ after grinding).

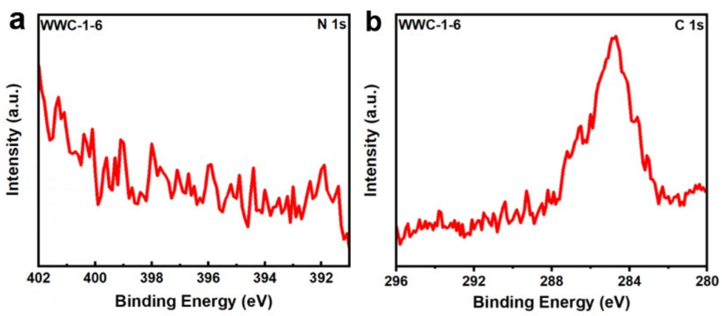

Fig. S12. (a) N 1s and (b) C 1s XPS spectra of WWC-1-6 heterostructures.

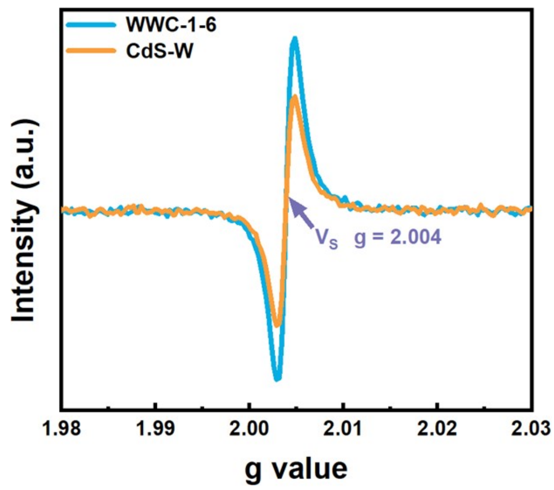

Fig. S13. EPR spectra of 1T-WS_2/2H-WS_2/CdS heterostructures (WWC-1-6) and CdS-W (CdS-W represents only calcination the mixture of CdS and $H_{28}N_6O_{41}W_{12}{\cdot}H_2O$ after grinding).

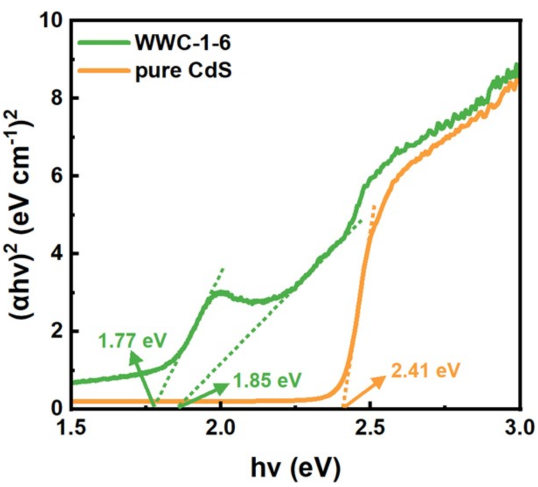

Fig. S14. Optical bandgaps of 1T-WS_2/2H-WS_2/CdS heterostructures (WWC-1-6) and pure CdS nanorods.

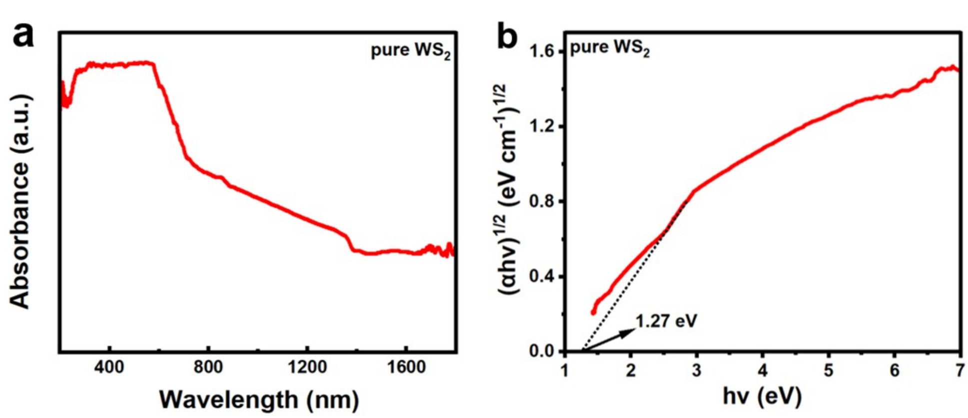

Fig. S15. (a) Ultraviolet-visible absorption spectrum and (b) optical bandgap of pure WS_2 nanosheets.

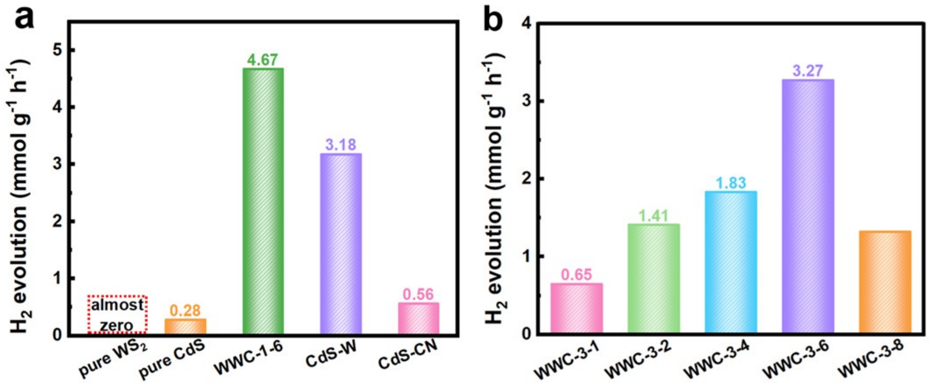

Fig. S16. H_2 evolution rates of (a) different catalysts and (b) 1T-WS_2/2H-WS_2/CdS heterostructures (WWC-3-1, WWC-3-2, WWC-3-4, WWCp-3-6, WWC-3-8).

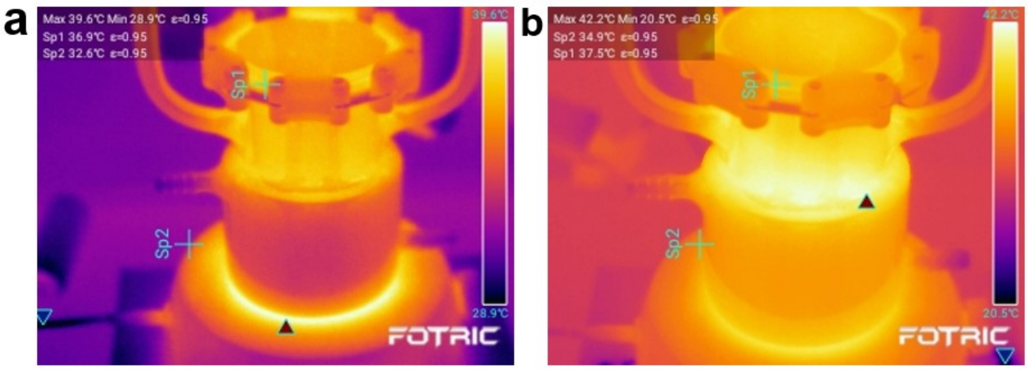

Fig. S17. The highest temperature of photocatalytic system with (a) pure CdS and (b) WWC-1-6 as photocatalysts without cooling water.

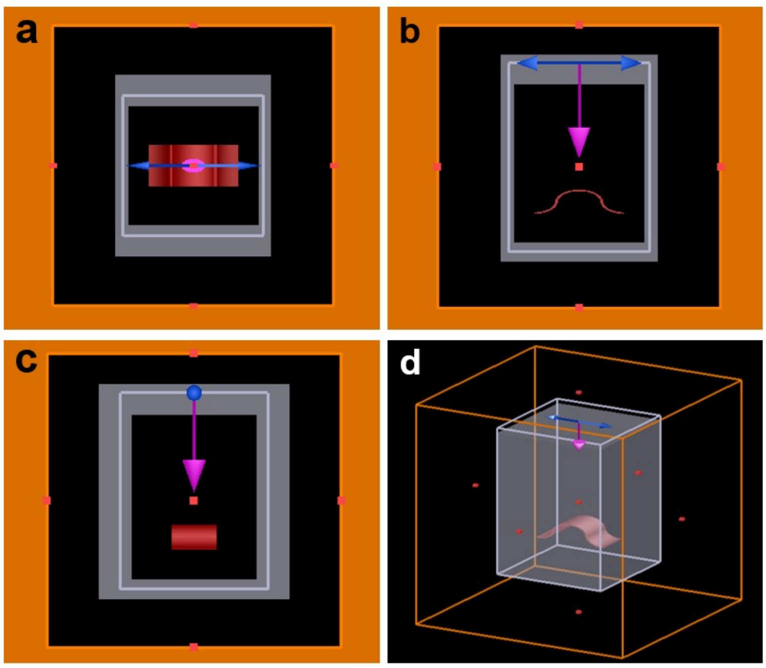

Fig. S18. (a) XY direction, (b) XZ direction, (c) YZ direction, and (d) 3D modeling of FDTD simulation diagram of WS_2 nanosheets.

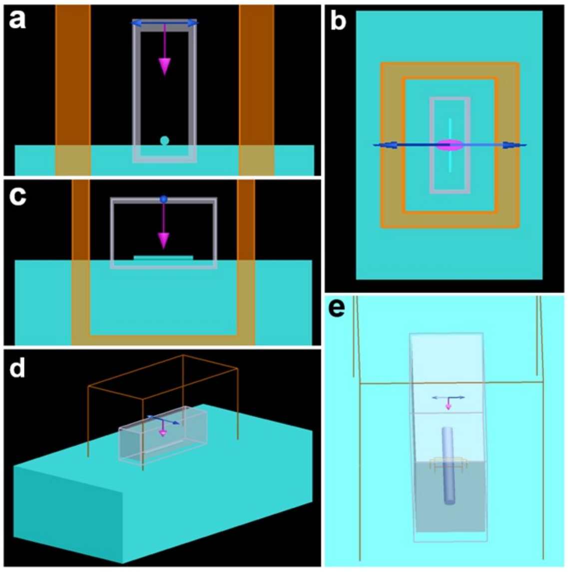

Fig. S19. (a) XZ direction, (b) XY direction, (c) YZ direction, and (d, e) 3D modeling of FDTD simulation diagram of CdS nanorods.

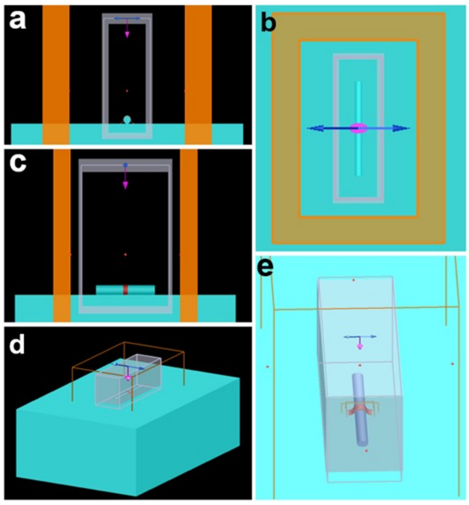

Fig. S20. (a) XZ direction, (b) XY direction, (c) YZ direction, and (d, e) 3D modeling of FDTD simulation diagram of 1T-WS_2/2H-WS_2/CdS heterostructures.

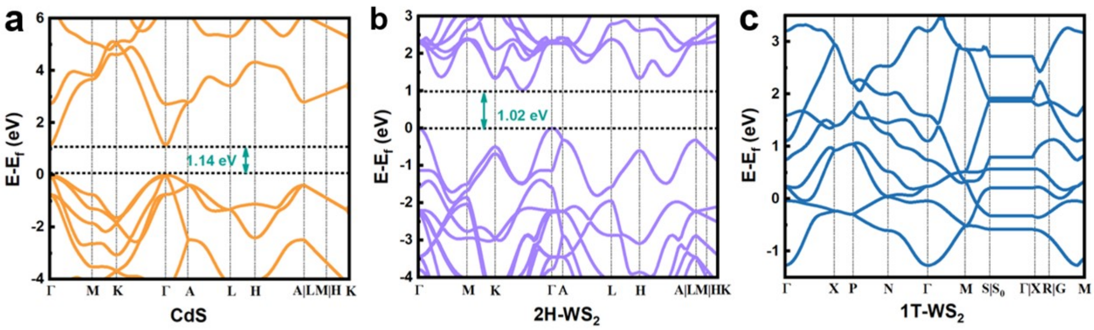

Fig. S21. Theoretically calculated bandgap of (a) CdS, (b) 2H-WS_2, and (c) 1T-WS_2.

Table S1. Specific dosage and the corresponding sample designations.

The mass ratio	$H_{28}N_6O_{41}W_{12}\cdot H_2O$	$C_2H_4N_4$	sample designations
1:1	0.01 g	0.01 g	WWC-1-1
	0.02 g	0.02 g	WWC-1-2
	0.04 g	0.04 g	WWC-1-4
	0.06 g	0.06 g	WWC-1-6
	0.08 g	0.08 g	WWC-1-8
1:3	0.01 g	0.03 g	WWC-3-1
	0.02 g	0.06 g	WWC-3-2
	0.04 g	0.12 g	WWC-3-4
	0.06 g	0.18 g	WWC-3-6
	0.08 g	0.24 g	WWC-3-8

Table S2. Quantitative analyses of the fitted XPS peaks of 1T-WS_2 and 2H-WS_2.

WWC-1-6	2H phase	Peaks BE (eV)	35.02	32.66
		Area	10787.43	13683.78
	1T phase	Peaks BE (eV)	34.18	31.95
		Area	6930.8	8791.84
WWC-3-6	2H phase	Peaks BE (eV)	35.12	32.98
		Area	11220.54	14265.61
	1T phase	Peaks BE (eV)	34.09	31.87
		Area	2844.80	3573.97

For WWC-1-6:

$$[1T]\% = \frac{[1T]}{[1T]+[2H]} \times 100\% = \frac{15722.64}{15722.64+24471.21} \times 100\% = 39.12\%$$

For WWC-3-6:

$$[1T]\% = \frac{[1T]}{[1T]+[2H]} \times 100\% = \frac{6418.77}{6418.77+25486.15} \times 100\% = 20.11\%$$

Table S3. Photocatalytic hydrogen production performance of photocatalysts reported in literatures.

Photocatalysts	H_2 (mmol/g/h)	Illumination	Sacrificial agent	Ref.
CdS/g-C_3N_4	0.392	3 W LED (full spectrum)	20% CH_3OH	1
CdS/TiO_2	1.5	300 W Xe lamp (>420 nm)	0.5 M Na_2S and 0.5 M Na_2SO_3	2
CdS/Ti_3C_2	2.407	300 W Xe lamp (>420 nm)	10 wt% lactic acid solution	3
CdS/g-C_3N_4	4.15	300 W Xe lamp (>400 nm)	0.35 M Na_2S and 0.25 M Na_2SO_3	4
CdS/Ti^{3+}/N-TiO_2	1.118	300 W Xe lamp (>420 nm)	0.35 M Na_2S and 0.25 M Na_2SO_3	5
CdS/Cu_2O/g-C_3N_4	1.84	300 W Xe lamp (AM 1.5G)	20% CH_3OH	6
NiS/CdS	2.18	300 W Xe lamp (>420 nm)	0.35 M Na_2S and 0.25 M Na_2SO_3	7
NiS/CdS	0.15	300 W Xe lamp (>420 nm)	10 wt% lactic acid solution	8
CdS/g-C_3N_4/CuS	1.15	300 W Xe lamp (>420 nm)	0.35 M Na_2S and 0.25 M Na_2SO_3	9
CdS/Co-MoS_x	0.54	300 W Xe lamp (>420 nm)	10 wt% lactic acid solution	10
1T-WS_2/2H-WS_2/CdS	**4.67**	**300 W Xe lamp (>420 nm)**	**0.35 M Na_2S and 0.25 M Na_2SO_3**	**This work**

Table S4. Carrier densities of pure CdS and 1T-WS_2/2H-WS_2/CdS heterostructures (WWC-1-6 and WWC-3-6).

Samples	Carrier density cm^{-3}
pure CdS	7.16×10^{18}
WWC-1-6	1.78×10^{19}
WWC-3-6	1.45×10^{19}

Table S5. Time-resolved PL decay curve parameters obtained by double-exponential function simulation.

Samples	τ_1 (ns)	τ_2 (ns)	A_1 (%)	A_2 (%)	τ_{av} (ns)
pure CdS	1.12	10.13	66.22	33.78	4.16
pure WS_2	1.52	17.61	64.52	35.48	7.23
WWC-1-6	1.38	12.13	63.93	36.07	5.25

REFERENCES

1. Z. Li, L. Zhang, Y. Liu, C. Shao, Y. Gao, F. Fan, J. Wang, J. Li, J. Yan, R. Li and C. Li, Surface-Polarity-Induced Spatial Charge Separation Boosts Photocatalytic Overall Water Splitting on GaN Nanorod Arrays, Angew. Chem. Int. Ed., 2020, **132**, 945-952.
2. Z. Jiang, K. Qian, C. Zhu, H. Sun, W. Wan, J. Xie, H. Li, K. Wong and S. Yuan, Carbon nitride coupled with CdS-TiO_2 nanodots as 2D/0D ternary composite with enhanced photocatalytic H_2 evolution: a novel efficient three-level electron transfer process, Appl. Catal. B, 2017, **210**, 194-204.
3. R. Xiao, C. Zhao, Z. Zou, Z. Chen, L. Tian, H. Xu, H. Tang, Q. Liu, Z. Lin and X. Yang, In situ fabrication of 1D CdS nanorod/2D Ti_3C_2 MXene nanosheet Schottky heterojunction toward enhanced photocatalytic hydrogen evolution, Appl. Catal. B, 2020, **268**, 118382.
4. J. Zhang, Y. Wang, J. Jin, J. Zhang, Z. Lin, F. Huang and J. Yu, Efficient visible-light photocatalytic hydrogen evolution and enhanced photostability of core/shell CdS/g-C_3N_4 nanowires, ACS Appl. Mater. Interfaces, 2013, **5**, 10317-10324.
5. Y. Qin, H. Li, J. Lu, F. Meng, C. Ma, Y. Yan and M. Meng, Nitrogen-doped hydrogenated TiO_2 modified with CdS nanorods with enhanced optical absorption, charge separation and photocatalytic hydrogen evolution, Chem. Eng. J., 2020, **384**, 123275.
6. F. Nekouei, S. Nekouei, M. Pouzesh and Y. Liu, Porous-CdS/Cu_2O/graphitic-C_3N_4 dual pn junctions as highly efficient photo/catalysts for degrading ciprofloxacin and generating hydrogen using solar energy, Chem. Eng. J., 2020, **385**, 123710.
7. W. Zhang, Y. Wang, Z. Wang, Z. Zhong and R. Xu, Highly efficient and noble metal-free NiS/CdS photocatalysts for H_2 evolution from lactic acid sacrificial solution under visible light, ChemComm, 2010, **46**, 7631-7633.
8. C. Li, H. Wang, S. Naghadeh, Z. Zhang and P. Fang, Visible light driven hydrogen evolution by photocatalytic reforming of lignin and lactic acid using one-dimensional NiS/CdS nanostructures, Appl. Catal. B, 2018, **227**, 229-239.
9. F. Cheng, H. Yin and Xiang Q, Low-temperature solid-state preparation of ternary CdS/g-C_3N_4/CuS nanocomposites for enhanced visible-light photocatalytic H_2-production activity, Appl. Surf. Sci., 2017, **391**, 432-439.
10. Y. Lei, J. Hou, F. Wang, X. Ma, Z. Jin, J. Xu and S. Min, Boosting the catalytic performance of MoS_x cocatalysts over CdS nanoparticles for photocatalytic H_2 evolution by Co doping via a facile photochemical route, Appl. Surf. Sci., 2017, **420**, 456-464.